New Journal of Physics
An Institute of Physics and Deutsche Physikalische Gesellschaft Journal

Zonal flow generation in the improved confinement mode plasma and its role in confinement bifurcations

M G Shats and W M Solomon

Plasma Research Laboratory, Research School of Physical Sciences and Engineering, Australian National University, Canberra 0200, Australia
E-mail: Michael.Shats@anu.edu.au

New Journal of Physics **4** (2002) 30.1–30.14 (http://www.njp.org/)
Received 1 March 2002, in final form 9 May 2002
Published 29 May 2002

Abstract. Unstable fluctuations develop in the initially quiescent plasma in the improved confinement mode of the H-1 heliac when the radial electric field (E_r) shear exceeds some critical value. These unstable E_r shear-driven modes are shown to generate zonal-flow-like poloidally symmetric potential structures, similar to those generated in the low confinement mode (Shats M G and Solomon W M 2002 *Phys. Rev. Lett.* **88** 045001). The structures modulate their parent waves, the background E_r shear and the fluctuation-driven radial transport. The onset of zonal flows is observed as a precursor to the plasma confinement bifurcation to an even higher confinement regime.

1. Introduction

The generation of zonal flows (ZFs) in toroidal plasma has been a focus of active research in recent years. ZFs are turbulence-generated poloidally symmetric low-frequency potential structures [1], which can play an important role in the turbulence self-regulation [2]. In such a system [2], drift wave turbulence nonlinearly generates ZFs, which in turn modulate the drift wave amplitude and control the turbulence level through a random shearing process. Turbulent transport also appears to be modulated by ZFs, exhibiting bursts at the ZF frequency as has been demonstrated in simulations [3], theory [4] and experiment [5]. ZF-like structures have recently been observed [5] in the H-1 heliac. It has been demonstrated that these structures, seen as low-frequency fluctuations in the plasma potential, have zero poloidal wavenumbers k_θ, finite radial wavenumbers k_r, $(k_r \gg k_\theta \sim 0)$ and are generated through a three-wave interaction process in various modes of confinement in the H-1 heliac.

PII: S1367-2630(02)34410-0
1367-2630/02/000030+14$30.00

Fluctuations in the low confinement mode in H-1 have been identified as unstable pressure-gradient-driven (PGD) modes [6], which drive a substantial radial flux of particles, thus affecting the plasma confinement. It has been discovered recently that the fluctuation-driven transport in H-1 is non-ambipolar [7]. Electrons are transported radially by fluctuations approximately ten times more efficiently than ions, which results in a fluctuation-driven radial current. This current is capable of significantly modifying the radial electric field, and through it, the particle confinement, which has been demonstrated in the H-1 experiments [7]. Since fluctuations generate ZFs and ZFs change the radial electric field in the plasma, which has been found to be the most essential ingredient in the confinement bifurcations observed in H-1 [8], it is important to investigate the generation of ZFs and their role in confinement jumps in various plasma conditions.

In this paper we present experimental results on the generation of ZF-like structures in the improved confinement mode (H-mode) and on the role of these structures in the confinement bifurcations. In particular, it is shown that:

1. the role played by fluctuations during the confinement transitions varies in different confinement modes in H-1. It is possible that fluctuations are not a necessary ingredient in the confinement bifurcations, though they can trigger a transition or can modify its dynamics. The bifurcations themselves may be similar to those discussed in the literature with regard to stellarators (see, for example, [9, 10, 11, 12]);
2. fluctuations that are sometimes observed in the H-mode plasma in H-1 [6, 13] have many features of the radial electric field shear-driven modes [14, 15, 16];
3. these shear-driven fluctuations can become unstable and can generate ZF-like structures;
4. the development of such structures is often correlated with a confinement bifurcation and may be considered as a candidate for the confinement bifurcation trigger or precursor.

The paper is organized as follows. In section 2 we describe experimental conditions and types of confinement bifurcations in the low-temperature plasma in the H-1 heliac. In section 3 we describe characteristics of fluctuations in the high confinement mode and the results on the ZF generation. In section 4 we discuss and summarize the results.

2. Plasma conditions and confinement modes in the H-1 heliac at low magnetic field

All results discussed in this paper were obtained in the H-1 heliac [17], a helical axis stellarator having a major radius of $R_0 = 1.0$ m and a minor plasma radius of <0.2 m. The magnetic field structure of H-1 is characterized by a relatively high rotational transform ($\iota = 1.1$–1.5 in the described experiments) and very low global magnetic shear ($\hat{s} = (\rho/\iota)(\mathrm{d}\iota/\mathrm{d}\rho) \approx 0.005$–$0.01$).

In the experiments discussed here, H-1 was operated at low magnetic fields (<0.2 T) with current-free plasma produced by the pulsed radio-frequency (rf) power of <100 kW at 7 MHz. The rf power pulse length is about 80 ms. The electron temperature in the discharge is low enough ($T_e = 5$–40 eV) so that a number of electric probes can be inserted as far as the magnetic axis. The experiments are performed in argon, which gives typically more reproducible discharges, and are less affected by the insertion of the probes. The ion temperature, as measured using the electrostatic ion energy analyser (which has also been confirmed by spectroscopic Doppler broadening measurements) is in the range between 20–60 eV [21]. Together with the large ion

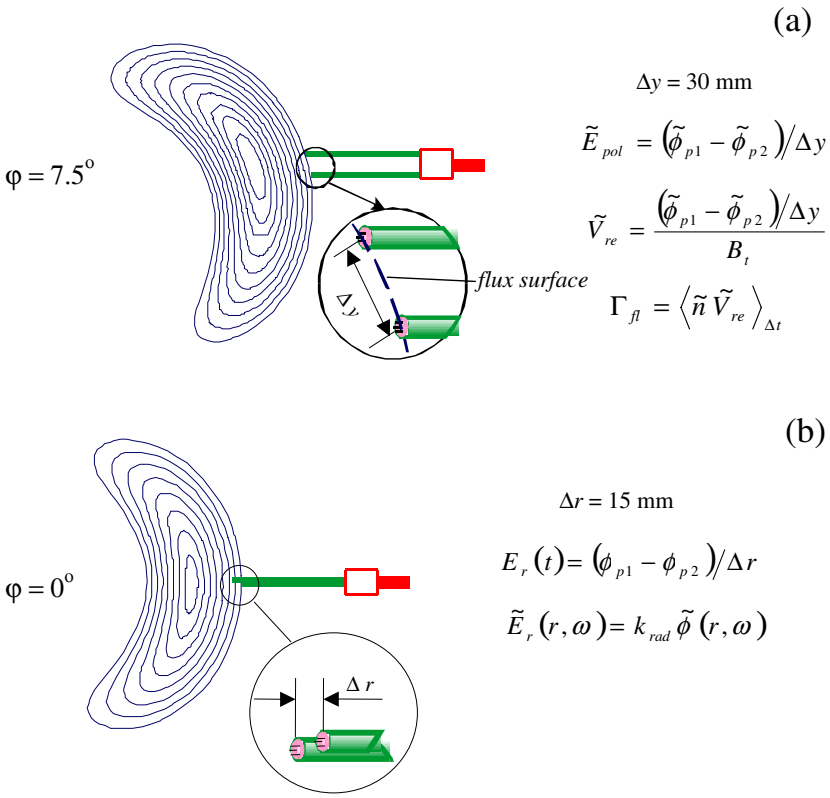

Figure 1. Schematic diagrams of the probe geometry: (a) the poloidal fork probe and (b) the radial fork probe.

mass ($m_i = 40m_p$, where m_i is the ion mass and m_p is the proton mass) and the low magnetic field this brings the ion Larmor radius into the range of $\rho_i = 3$–5 cm.

Fluctuations in the plasma electrostatic potential and electron density are studied using various combinations of the triple probes. Each triple probe [18] is capable of measuring the ion saturation current I_s, the plasma potential V_p, and the electron temperature T_e with a time resolution of about 1 ms (limited by the acquisition rate of 1 MHz). In the reported experiments two pairs of triple probes have been employed to measure fluctuations in the poloidal and the radial electric field, as well as the fluctuation-driven particle flux. The probe set-up is shown in figure 1. Two triple probes separated poloidally by $\Delta y = 30$ mm (figure 1(a)) allow measurements of the poloidal electric field, while two probes separated radially by $\Delta r = 15$ mm (figure 1(b)) are used to measure the radial electric field and its fluctuations. To avoid the cross-coupling of the poloidal and radial components of the electric field, all four probes have been aligned with respect to the same flux surface using the electron beam mapping technique. Note that this is possible in a stellarator, such as H-1, where the vacuum magnetic flux surfaces practically coincide with the low-pressure plasma magnetic surfaces. Two radially displaced triple probes are positioned ± 7.5 mm on either side of the flux surface to which two poloidally separated probes are aligned. To avoid shadowing of one of the radial probes by the other along the magnetic field lines, the two probes are also slightly displaced poloidally ($\sim$3–4 mm). Such displacement introduces a phase shift. By rotating the radial pair of probes with respect to the midplane of the machine to

change this poloidal separation in the range of 0–15 mm, it was found that the phase shift due to the poloidal separation is negligibly small compared with the radial phase shift.

Several different types of confinement bifurcations have been observed in the low-temperature plasma in the H-1 heliac. It has been shown, similarly to other toroidal experiments, that the radial electric field plays a very important role in these bifurcations [6, 8]. This role though is not exactly what has been proposed for other experiments (see, for example, [19]). In particular, our understanding of the role of turbulence in the H-1 heliac has been substantially revised in the light of the following. Firstly, the fluctuation-driven transport was found to be able to reverse radially [6, 7, 13], so that the suppression of fluctuations appears to be not the only option for the modification in the turbulent transport. Secondly, it has been found that the particle transport produced by fluctuations in H-1 is not ambipolar [7]. When the mean E_r shear exceeds some critical value, fluctuations are suppressed, in agreement with the shear suppression model, and the fluctuation-driven radial current is turned off. This leads to even further shearing in E_r, which secures the transition. Thirdly, fluctuations in H-1 have been found to be able to nonlinearly generate time-varying poloidally symmetric $\tilde{E} \times B$ structures [5]. Such structures show many signatures of ZFs and are essentially slow time-varying radial electric fields. Thus, fluctuations in H-1 can linearly generate a mean radial electric field (through the radial non-ambipolar transport) and also can nonlinearly generate time-varying E_r.

Here we briefly discuss these confinement bifurcations observed in H-1. Figure 2 shows an example of a spontaneous transition from low to high mode. This type of transition has been studied in [6, 7, 20, 21]. Here we summarize the findings. In the low confinement mode, the plasma is dominated by strong quasi-coherent fluctuations, which have been identified as unstable PGD modes (poloidal mode numbers $m = 1$–4). These fluctuations in the plasma potential and density generate substantial particle flux [6]. It has also been shown that electrons are transported radially by fluctuations approximately ten times more efficiently than ions, such that fluctuations effectively drive a radial current [7]. The non-ambipolarity is likely to be due to the finite ion Larmor radius (FLR) effect [22, 23] since for these fluctuations $k_\perp \rho_i > 1$. This current, along with other bipolar loss processes, affects the radial electric field. It is found that the radial electric field in L-mode is always less sheared than in H-mode. The fluctuation-driven radial current seems to flatten the E_r profile, as shown in figure 2(c), as if fluctuations resist the formation of the strong E_r shear that would lead to their suppression. When a sufficiently high E_r shear is formed in the plasma (as discussed in [8]), fluctuations are suppressed, resulting in considerably more sheared E_r, as shown in figure 2(c). The average electron density jumps by a factor of two across the transition (figure 2(a)), while the fluctuations are suppressed (figure 2(b)). The new steady state is characterized by more peaked plasma pressure profiles, reduced anomalous transport and sheared radial electric field. It has been found that, in the range of low magnetic fields described here ($B < 0.15$ T), the magnetic field strength B appears to be the strongest external parameter (but not the only one) affecting the radial electric field and its shear (for details, see [8]). The bifurcations reported here were observed during a magnetic field scan in the H-1 heliac in the rf-produced argon plasma. The threshold E_r shear for the suppression of the L-mode fluctuations is found to be $|E_r'| > (30\text{–}40)$ kV m^{-2}.

Above some critical B (in fact above some critical E_r shear), fluctuations are suppressed in H-mode. This mode of confinement is referred to as 'quiescent' H-mode, or H_q-mode. When the magnetic field is further increased, the plasma may experience another bifurcation to even higher electron density and more peaked n_e profiles. An example of such a bifurcation is shown in figure 3. The line-average density is increased across the transition by $\sim$30% as seen in

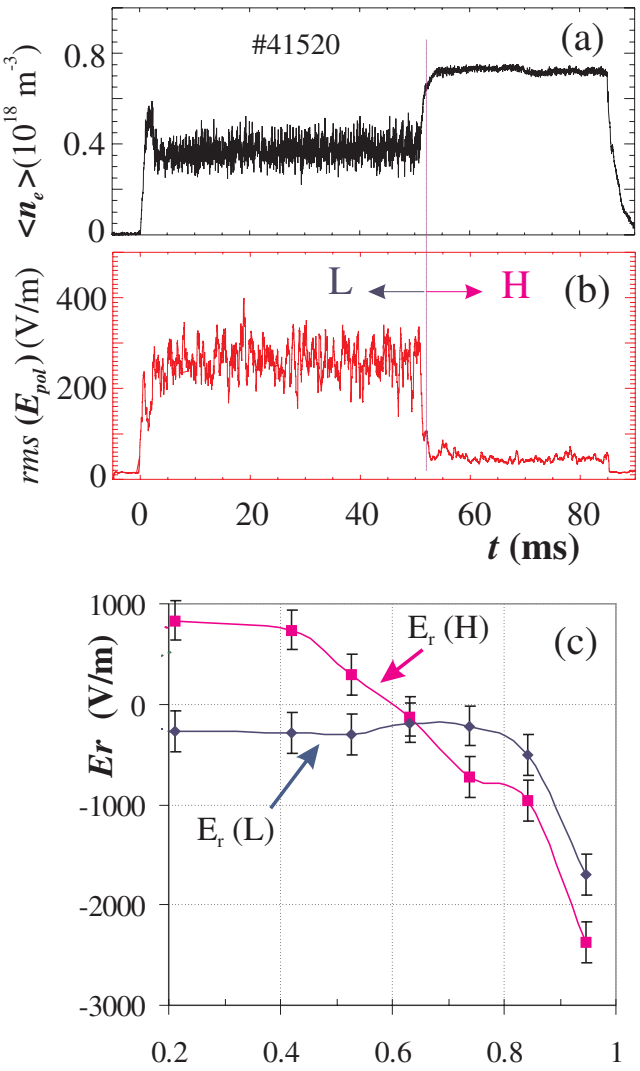

Figure 2. Time evolution of (a) the line-average density and (b) the rms of the fluctuations in the poloidal electric field during the discharge showing spontaneous transition from low to high confinement modes. (c) Radial profiles of the mean radial electric field in low (diamonds) and high (squares) modes.

figure 3(a). The radial electric field changes across the transition to become even more sheared in the higher confinement mode, as illustrated in figure 3(c). The E_r shear before the bifurcation is about $E_r' \approx 50$ kV m^{-2}, similar to E_r' in the quiescent H-mode of figure 2(c). Such a shear exceeds the threshold E_r' for the suppression of the PGD modes observed in L-mode. After the bifurcation (at $t \geq 68$ ms), the E_r shear is increased to $E_r' \approx 60$ kV m^{-2}. As seen in figure 3(b), fluctuations in the poloidal electric field become unstable after about 20 ms. The fluctuation amplitude becomes modulated after $t \geq 40$ ms. It is likely that fluctuations observed in the high confinement regimes in H-1 are the modes driven by the gradient in the radial electric field [14, 15, 16]. The properties of the fluctuations and the development of the low-frequency instability seen in figure 3(b) after $t \sim 40$ ms are described in detail in section 3. We refer to the improved confinement mode where fluctuations are observed as 'fluctuating' H-mode, or H_{fl}

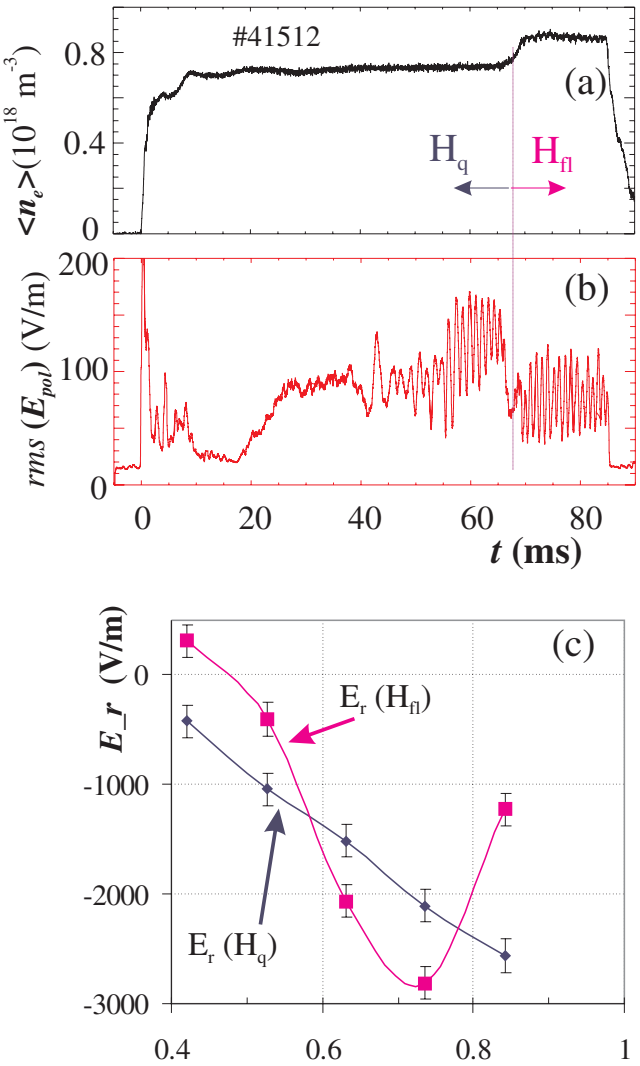

Figure 3. Time evolution of (a) the line-average density and (b) the rms of the fluctuations in the poloidal electric field during the discharge showing spontaneous transition from 'quiescent' to 'fluctuating' high confinement modes. (c) Radial profiles of the mean radial electric field in 'quiescent' (diamonds) and 'fluctuating' (squares) H modes.

mode. It should also be noted that this confinement mode is observed in the magnetic configuration characterized by very low magnetic shear in the H-1 heliac $\hat{s} = (\rho/\iota)(\mathrm{d}\iota/\mathrm{d}\rho) \approx 0.006$, where $\rho = r/a$ and ι is the rotational transform (inverse safety factor).

3. ZF instability in H-mode and confinement transition

As mentioned above, fluctuations observed in the H-mode plasma (figure 3) appear when the E_r shear far exceeds the threshold for the fluctuation suppression in L-mode and are observed in the radial plasma region of the maximum E_r'. We can distinguish three different confinement modes depending on the E_r shear as follows. In L-mode, dominated by the PGD fluctuations,

the E_r shear is less than the threshold for the fluctuation suppression, $E_r' < 30$ kV m^{-2}. In the quiescent H-mode, the E_r shear is in the range $30 < E_r' < 50$ kV m^{-2} (H$_q$-mode). Finally, in fluctuating H-mode, the E_r shear-driven (ESD) modes become unstable when $E_r' > 50$ kV m^{-2}. The development of a new instability is observed in this range of E_r'.

As seen in figure 3(b), the onset of fluctuations in H-mode (at $t \sim 20$ ms) is followed by a strong low-frequency modulation of the fluctuation amplitude after $t \sim 45$ ms. This low-frequency instability is followed by the plasma bifurcation at $t \sim 66$ ms. The line-average density is increased by $\sim$30% across the transition (figure 3(a)), while the low-frequency fluctuations ($\sim$1 kHz) are stabilized at a high level. Frequency spectra of fluctuations are shown in figure 4 for the same discharge as in figure 3. After the onset of the fluctuations ($t = (42$–$54)$ ms), frequency spectra of both the poloidal and the radial electric fields are dominated by a narrow-band coherent feature at $f \sim 11.5$ kHz (figure 4(b)). These fluctuations have relatively high poloidal and radial wavenumbers (64 and 104 m^{-1} respectively). As the instability develops ($t = (54$–$66)$ ms) the frequency spectra become broader (figure 4(c)) and a low-frequency component of the plasma potential fluctuations with $f \sim 1$ kHz and $k_r \gg k_\theta$ develops in the plasma. After the bifurcation (figure 4(c)), at $t = (68$–$80)$ ms, the higher-frequency spectra ($f = 10$–16 kHz) become even broader, while the low-frequency feature stabilizes at a high level, again showing $k_r \approx 10k_\theta$.

It has been found that unstable fluctuations in H-1 can nonlinearly generate time-varying potential structures, which have many properties of ZFs [5]. In the presented spectra, two types of fluctuations are observed: higher-frequency (10–15 kHz) fluctuations which are relatively symmetric in the poloidal plane, $k_r \approx k_\theta$, and low-frequency ($f \sim 1$ kHz) fluctuations with $k_r \gg k_\theta$. The low-frequency anisotropic features in the fluctuation spectra may be generated by the higher-frequency fluctuations via three-wave interactions [5, 24]–[26]. It has been shown that the energy transfer between the smaller-scale fluctuations and larger-scale shear flows is proportional in our case to $\sum_{k=k_1+k_2} \mathrm{Re}[\langle \tilde{E}_r^*(k)\tilde{n}(k_1)\tilde{E}_\theta(k_2)\rangle]$, where $\tilde{E}_r^*(k)$ and $\tilde{E}_\theta(k_1)$ are fluctuations in the radial and poloidal electric fields (the asterisk denotes the complex conjugate), and $\tilde{n}(k_2)$ represents density fluctuations satisfying the wavenumber selection rule in the three-wave processes, $k = k_1 + k_2$. Changes in the degree of the nonlinear coupling between the three fluctuating quantities are reflected in the real part of the bispectrum $B_k(k_1, k_2) = \sum_{k=k_1+k_2}\langle \tilde{E}_r^*(k)\tilde{n}(k_1)\tilde{E}_\theta(k_2)\rangle$, or in the normalized bispectrum, the squared crossed-bicoherence, which is independent of the fluctuation amplitude

$$b_f^2(f_1, f_2) = \frac{|\langle E_{rad,f}^* n_{f_1} E_{\theta f_2}\rangle|^2}{\langle E_{rad,f} E_{rad,f}^*\rangle |\langle n_{f_1} E_{\theta f_2}^*\rangle|^2}, \tag{1}$$

where predictions for the k-domain are transformed to the frequency domain, so that the phase-coherent three-wave interaction obeys the frequency selection rule, $f = f_1 + f_2$. We also compute the summed cross-bicoherence (SCB) $SCB = \sum_{f=f_1+f_2} b_f^2(f_1, f_2)$, which gives a measure of the coherent three-wave coupling for all frequencies satisfying $f = f_1 + f_2$. Plots of the SCB are shown in figure 5 for the same three time intervals as the frequency spectra of figure 4. When the frequency spectra of the fluctuations are narrow ($t = 42$–54 ms), the level of the three-wave interaction is low (figure 5(b)). As the instability develops and the spectra become broader ($t = 54$–66 ms), the level of the SCB increases at both higher (10–12 kHz) and lower (0.8–1 kHz) frequencies, indicating stronger coupling between the modes, as seen in figure 5(c). After the bifurcation, at $t = 68$–80 ms, the nonlinear coupling remains strong (figure 5(d)).

To analyse the development of the low-frequency instability prior to the bifurcation we apply the wavelet analysis technique to the fluctuations in the poloidal electric field E_θ, radial electric

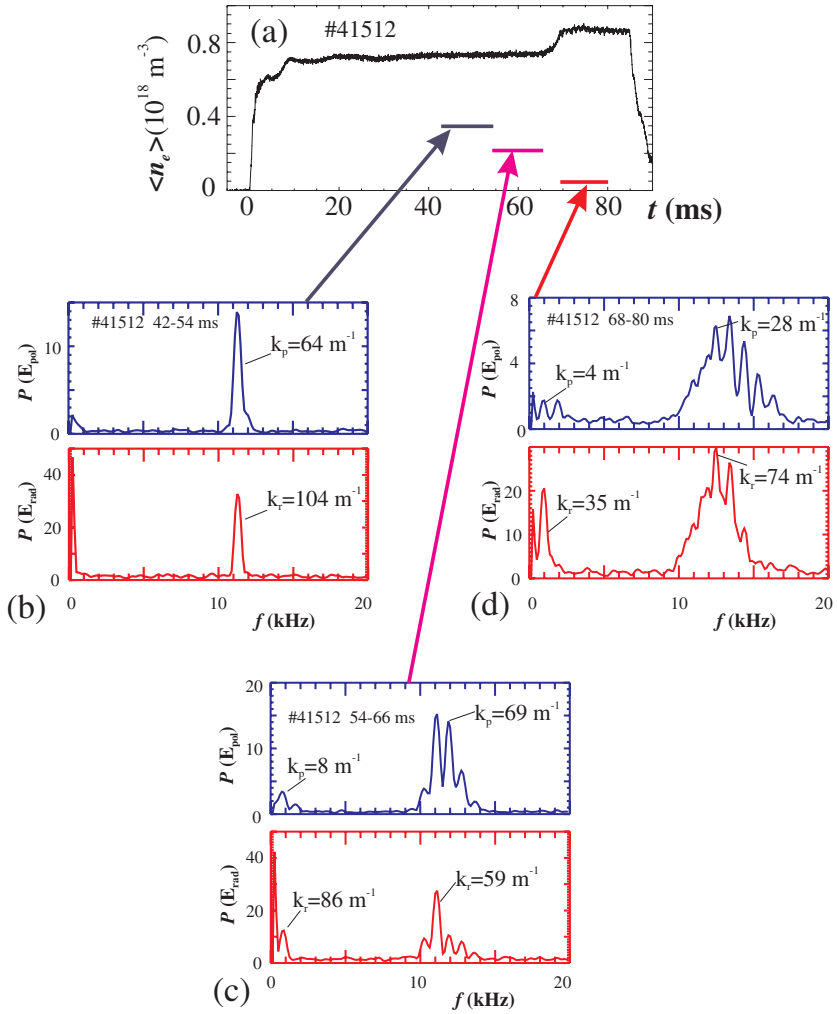

Figure 4. Time evolution of (a) the line-average density and frequency spectra of the fluctuations in the poloidal and radial electric fields for the discharge of figure 3 for three time intervals: (b) $t = 42$–54 ms, (c) $t = 54$–66 ms and (d) $t = 68$–80 ms.

field, E_r, and the time-resolved fluctuation-induced flux $\Gamma_{fl} = \langle \tilde{n}\tilde{V}_r \rangle = \langle \tilde{n}\tilde{E}_\theta \rangle / B_t$. Here we use the Morlet wavelet, which consists of a plane wave modulated by a Gaussian function [27]. The development of the low-frequency component in the radial electric field is seen in the raw signal of E_r (figure 6(b)) and even more clearly in the wavelet frequency–time plot of E_r in figure 6(c). As this $f \approx 0.8$ kHz feature develops at $t > 50$ ms, it starts modulating the higher-frequency ($\sim$11 kHz) fluctuations in the poloidal electric field shown in figure 6(d). The fluctuation-driven flux becomes 100%-modulated, as seen in figure 6(e). Note that the fluctuation-driven flux in this mode of confinement is radially inward (negative) in the region of $r/a = (0.4$–$0.7)$, as described in [6, 13].

We expect that, similar to L-mode, this flux is $>90\%$ non-ambipolar, i.e. fluctuations mainly drive radial electron fluxes. This is because the ion temperature is higher in H_{fl} mode than in L-mode [13]. Wavenumbers of the fluctuations are also higher in H_{fl} mode than in L-mode,

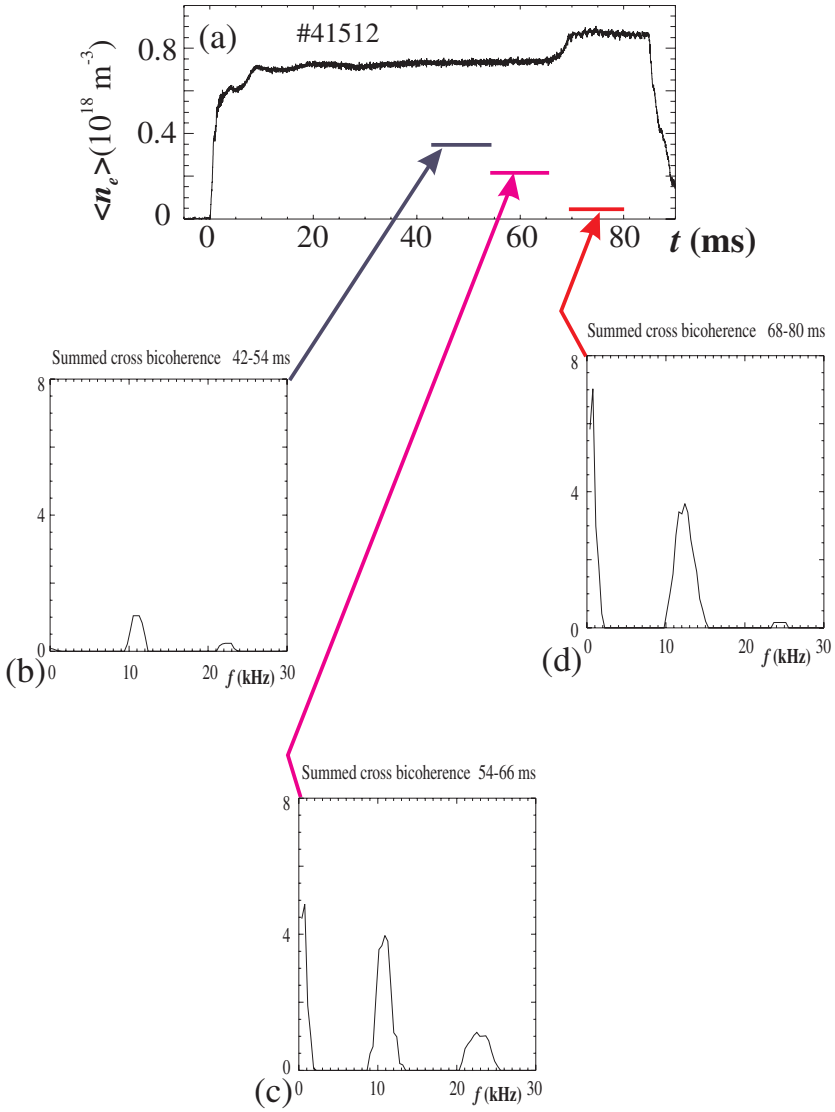

Figure 5. Plots of the cross-bicoherence (equation (1)) and the SCB for the same discharge as in figure 3 and the same time intervals as in figure 4.

$k_\perp = (80\text{–}120)$ m^{-1}, as seen in figures 4(b)–(d). Thus the FLR effect responsible for the non-ambipolarity of the fluctuation-driven transport should be stronger in H_{fl} mode $(k_\perp \rho_i = (4\text{–}6))$ than in L-mode $(k_\perp \rho_i \approx 2)$.

It is clear from figure 6 that the development of instability correlates with a substantial modulation in the fluctuation-driven radial current and large modulation in the radial electric field, and perhaps of its shear, since large fluctuations in E_r at $\sim$1 kHz are localized radially.

The evolution of the line-average electron density and of the radial electric field at $r/a \approx 0.42$ across the confinement transition is shown in figure 7. Although E_r changes across the transition, it does not lead with respect to n_e. Any significant change in E_r is observed at least 1 ms after n_e starts rising. However, the instance when n_e starts rising coincides with the moment when E_r reaches its most positive value after more than ten periods of the low-frequency

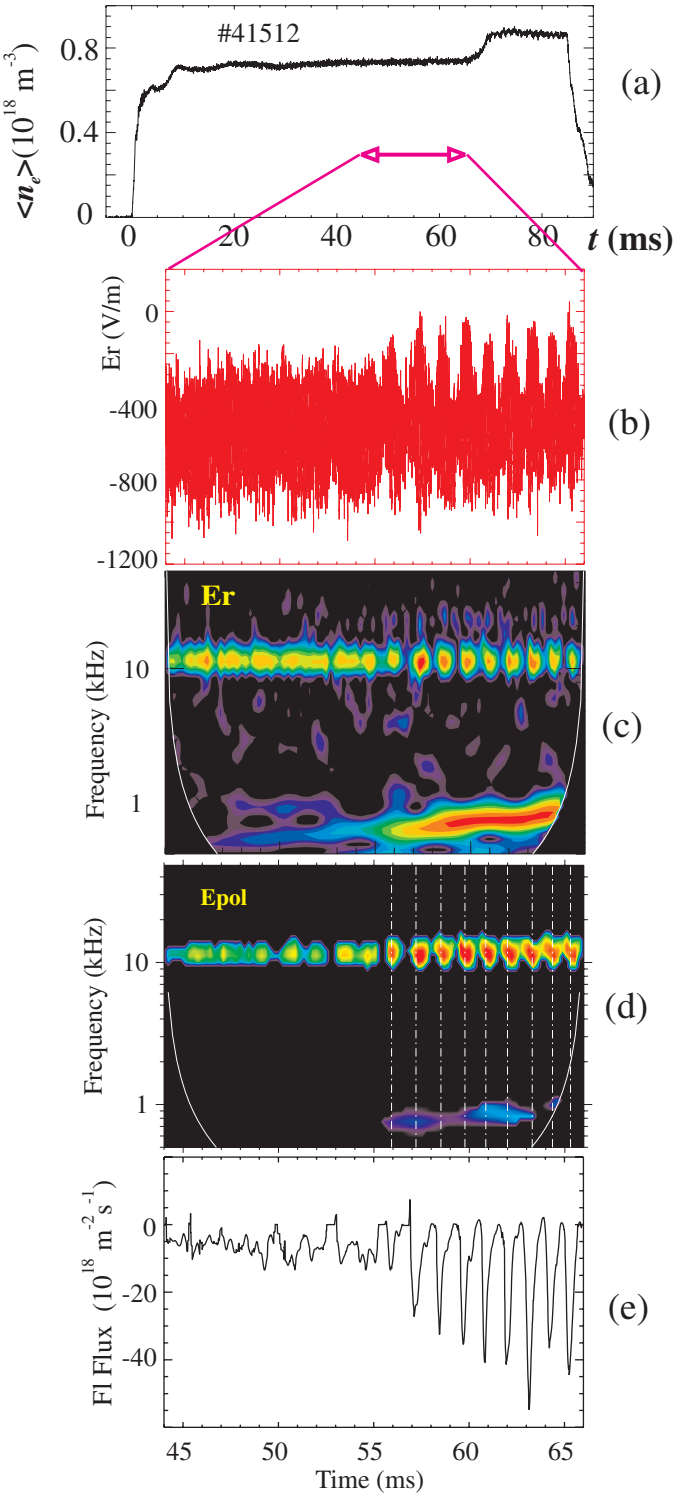

Figure 6. Time evolution of (b) the radial electric field at $r/a = 0.45$, frequency–time wavelet plots of the fluctuations in the (c) radial and (d) poloidal electric fields and (e) the frequency integrated fluctuation-driven particle flux for the discharge of figure 3 just before the confinement bifurcation. Negative flux corresponds to the radially inward particle transport.

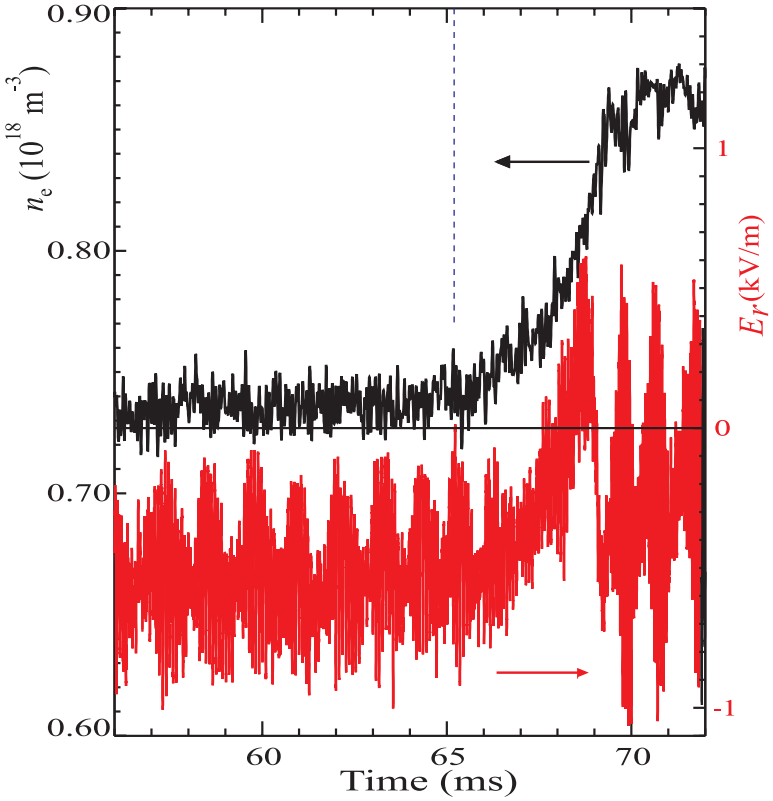

Figure 7. Time evolution of the plasma line-average density and the radial electric field before the bifurcation.

instability at $t \sim 65.3$ ms in figure 7. The radial electric field 'slowly' ($\sim$2 ms) changes until n_e reaches $\sim$90% of its new steady level and then bifurcates very quickly to a higher mode level. Observations that E_r never leads n_e on the slower timescale during the transition, and that E_r bifurcates to a steady-state level after n_e has almost reached its maximum, have also been confirmed at different radial positions in the range of $r/a \approx 0.4$–0.8.

4. Discussion and conclusions

It is found that the onset of fluctuations in H-mode correlates with the formation of the shear in the radial electric field exceeding a threshold of $|E_r'| \sim 50$ kV m^{-2}. Fluctuations are localized in the radial region of the largest E_r'. Such an E_r shear is well above the critical E_r' for the suppression of the PGD modes observed in L-mode. Also, unlike their L-mode counterparts, fluctuations in H-mode are only observed in the magnetic configuration with the lowest magnetic shear. It is reasonable to suggest that the H-mode fluctuations are the radial electric field shear-driven modes.

The observation of fluctuations in H-mode is not unique to H-1. The 'recovery' of fluctuations in H-mode has been reported in tokamaks, for example, [28, 29]. Properties of fluctuations in H-mode are found to be somewhat different than in L-mode; they are 'more coherent' and are localized to the strong radial electric field region. The background broadband turbulence is, however, noticeably reduced compared with the L-mode level [28]. It is possible

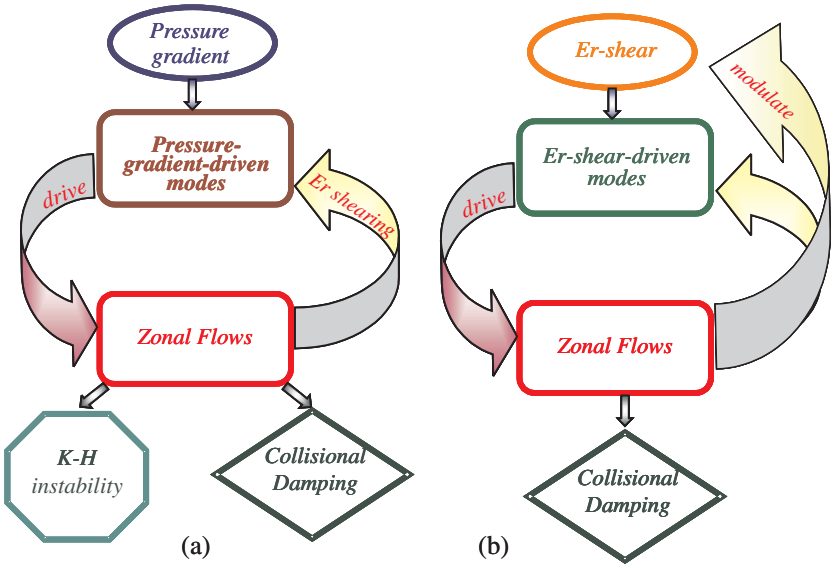

Figure 8. Schematic diagrams of the fluctuation–ZF interaction in (a) low and (b) high confinement modes.

that the $E \times B$ velocity shear-driven instability could develop in the high confinement mode, in the plasma region where E_r shear is strong enough to suppress PGD modes.

The radial electric field shear-driven turbulence has been observed in the edge plasma of the TEXT tokamak [14] and has been studied analytically [15] and numerically [16]. It has been shown that the sheared radial electric field drives symmetric (in k_r, k_θ space) wavenumber spectra. It has also been found that this turbulence is suppressed by the magnetic shear [15, 16]. Indeed, the ESD instability is not always observed in high E_r shear plasma regions if the magnetic shear is large [30], and it is not observed in the higher magnetic shear conditions in the H-1 heliac.

The ESD and Kelvin–Helmholtz (K–H) instabilities have recently been a focus of a number of theoretical studies in the context of ZF stability. Unstable K–H modes driven by ZFs have been suggested as the ZF damping mechanism [31] at low collisionality. In [32], the stability of ZFs have been modelled for the conditions of the negative magnetic shear tokamak plasma. It has been found that ZFs driven by the electron temperature gradient (ETG) modes are generated in the finite magnetic shear regions on both sides around the q_{min}-surface. These ZFs substantially reduce the electron thermal transport due to the ETG turbulence. In the region of low magnetic shear (in the vicinity of the q_{min}-surface) the K–H modes become unstable and damp ZF. It has been demonstrated that it is possible to control ZF by changing the magnetic shear, which strongly affects the stability of the K–H modes.

In the described examples the energy reservoir is the pressure gradient. It drives unstable drift waves, which generate ZFs through nonlinear mode coupling. This is schematically illustrated in figure 8(a). ZFs are damped either by collisions or give their energy to K–H modes. In the experiments reported here, the situation is somewhat different. ZFs are generated by the unstable ESD modes rather than the PGD modes, since $E'_{r\ sup} < E'_{r\ KH}$. Here $E'_{r\ sup}$ is the critical E_r shear for the suppression of the PGD modes and $E'_{r\ KH}$ is the threshold E_r shear needed for the ESD mode excitation. After ZFs develop, they modulate the mean radial electric field and its shear, thus modulating the energy reservoir for the ESD modes. This is schematically illustrated in figure 8(b).

ZF generation by the ESD modes discussed in this paper often precedes plasma bifurcations of the type illustrated in figures 3–7. The flux shown in figure 6(e) $\Gamma_{e,fl} \approx 10^{19}$ m^{-2} s^{-1} at $t \sim 50$ ms is $<10\%$ of the net particle flux estimated from the ionization balance. Considering that the ion part of this flux is at least ten times lower (see estimates of the non-ambipolarity above), the ambipolar fraction of the particle-driven flux before the bifurcation is small and it is difficult to expect that the modifications to the particle transport of the order of 1% of the net particle flux could lead to a 30% increase in the line-average electron density seen in figure 3(a). The role of fluctuations in the transition is likely to be due to their effect on the radial electric field. It is possible that when E_r shear reaches some critical value a bifurcation in the neoclassical transport occurs, as discussed in [12]. In this case, fluctuations may not be responsible for the bifurcation but rather contribute to the formation of the critical E_r shear, $E'_{r\ crit}$. When E'_r is already close to $E'_{r\ crit}$, the development of ZFs may play the role of a trigger, as discussed in section 3. However, in some plasma conditions, confinement transitions in H-mode occur without any active influence of the fluctuations. Various confinement transitions observed in the H-1 heliac have a common feature: the radial electric field shear is increased across the transition.

In summary, ZF-like structures are generated in the H-mode plasma in the H-1 heliac after broadband fluctuations develop. These fluctuations are identified as unstable modes driven by the shear in the radial electric field. They are observed in the plasma region of the maximum E_r shear in the magnetic configurations with low magnetic shear. ZF-like structures are poloidally symmetric ($k_r \gg k_\theta \cong 0$ as seen in figure 4) and they are nonlinearly coupled to their parent fluctuations via three-wave interactions, as seen in figure 5. The development of ZFs is observed before plasma bifurcations to higher confinement. ZFs appear to be a plausible bifurcation trigger in such discharges. However, modifications to the fluctuation-driven particle transport seem to be insufficient for the observed improvement in the particle confinement. More likely, fluctuations and ZFs influence the radial electric field and its shear and, through it, affect the confinement. The similarity between ZF structures driven by the PGD modes in L-mode [5] and the ZFs driven by the ESD mode, described in this paper, may be indicative of the universality (instability independence) of the ZF formation mechanism.

Acknowledgment

The authors are indebted to P H Diamond for valuable comments and interesting discussions.

References

[1] Hasegawa A and Wakatani M 1987 *Phys. Rev. Lett.* **59** 1581
[2] Diamond P H *et al* 1998 *Plasma Physics and Controlled Nuclear Fusion Research 17th IAEA Fusion Energy Conf.* (*Yokohama, Japan, 1998*) (Vienna: International Atomics Energy Agency) p IAEA-CN-69/TH3/1
[3] Hallatschek K and Biskamp D 2001 *Phys. Rev. Lett.* **86** 1223
[4] Malkov M A, Diamond P H and Rosenbluth M N 2001 *Phys. Plasmas* **8** 5073
[5] Shats M G and Solomon W M 2002 *Phys. Rev. Lett.* **88** 045001
[6] Shats M G 1999 *Plasma Phys. Control. Fusion* **41** 1357
[7] Solomon W M and Shats M G 2001 *Phys. Rev. Lett.* **87** 195003
[8] Shats M G *et al* 1998 *Phys. Plasmas* **5** 2390
[9] Fujisawa A *et al* 2000 *Phys. Plasmas* **7** 4152

[10] Maassberg H *et al* 1993 *Plasma Phys. Control. Fusion* B **35** 319
[11] Stroth U *et al* 2001 *Phys. Rev. Lett.* **87** 195003
[12] Toda S and Itoh K 2001 *Plasma Phys. Control. Fusion* **43** 629
[13] Shats M G and Rudakov D L 1997 *Phys. Rev. Lett.* **79** 2690
[14] Ritz Ch P, Bengtson R D, Levinson S J and Powers E J 1984 *Phys. Fluids* **27** 2956
[15] Chiueh T, Terry P W, Diamond P H and Sedlak J E 1986 *Phys. Fluids* **29** 231
[16] Scott B D, Terry P W and Diamond P H 1988 *Phys. Fluids* **31** 1481
[17] Hamberger S M *et al* 1990 *Fusion Technol.* **17** 123
[18] Chen S and Sekiguchi T 1965 *J. Appl. Phys.* **36** 2363
[19] Burrell K H 1999 *Phys. Plasmas* **6** 4418
[20] Shats M G *et al* 1996 *Phys. Rev. Lett.* **77** 4190
[21] Shats M G *et al* 1997 *Phys. Plasmas* **4** 3629
[22] Waltz R E 1982 *Phys. Fluids* **25** 1269
[23] Stringer T E 1992 *Nucl. Fusion* **32** 1421
[24] Diamond P H *et al* 2000 *Phys. Rev. Lett.* **84** 4842
[25] Tynan G R *et al* 2001 *Phys. Plasmas* **8** 2691
[26] Moyer R A *et al* 2001 *Phys. Rev. Lett.* **87** 135001
[27] Torrence C and Compo G P 1998 *Bull. Am. Meteorol. Soc.* **79** 61
[28] Tynan G R *et al* 1994 *Phys. Plasmas* **1** 3301
[29] Moyer R A *et al* 1995 *Phys. Plasmas* **2** 2397
[30] Ritz Ch P, Lin H, Rhodes T L and Wootton A J 1990 *Phys. Rev. Lett.* **65** 2543
[31] Rogers B N, Dorland W and Kotschenreuther M 2000 *Phys. Rev. Lett.* **85** 5336
[32] Idomura Y, Wakatani M and Tokuda S 2000 *Phys. Plasmas* **7** 3551